Scientific Research Publishing

Open Journal of Safety Science and Technology, 2023, 13, 27-50
https://www.scirp.org/journal/ojsst
ISSN Online: 2162-6006
ISSN Print: 2162-5999

Review of Blast Waves Analysis, Design, Structural and Materials Responses

Ahmed K. Taha, A. Osman, M. S. Zahran*

Department of Civil Engineering, Military Technical College, Cairo, Egypt
Email: *m.s.zahran@mtc.edu.eg

How to cite this paper: Taha, A.K., Osman, A. and Zahran, M.S. (2023) Review of Blast Waves Analysis, Design, Structural and Materials Responses. *Open Journal of Safety Science and Technology*, **13**, 27-50.
https://doi.org/10.4236/ojsst.2023.132002

Received: May 6, 2023
Accepted: June 27, 2023
Published: June 30, 2023

Abstract

With the increasing threat of terrorism and the rapid development of technology, the probability of accidental explosions such as incident blasts, mine explosions and terrorist attacks has increased. So, protecting important structures against terroristic attacks is a very important topic as terrorist attacks have increased and developed a lot these days especially using blast loads. This study is Carried out to cover the historical background and extensive literature review of the available previous research works focusing on the blast environment characteristics, fundamentals of blast loading and description of the methods used to predict blast loadings. Moreover, the research also covers a literature review on the response of structures subjected to blast loads and material behavior considering high strain rates. Hence blast loading effects can be predicted and utilized in improving the design of important structures.

Keywords

Reinforced Concrete, Blast Waves, Numerical Simulation, Comp-B, Concrete Structures

1. Introduction

Structural buildings can be exposed to blast loadings including accidental gas explosions or terrorist attacks during their service life, which might cause heavy human and economic losses. Over the last several decades, there has been great interest shown by the military and other governmental agencies in designing structures to withstand blast loadings. A variety of protective techniques are developed against increasing accidental explosions and terrorist attacks [1] [2].

The entire chain involved in the design and construction of structures has shown keen interest in the performance assessment of existing as well as new ci-

vilian structures when subjected to blast loading due to the increase in the number of intentional and accidental blast events throughout the world.

Blast events produce short-duration high-magnitude loadings which can greatly influence structural blast response. When compared to conventional loads, the frequencies of explosive loads are usually much higher. The action applied to a structural member when subjected to an explosive detonation is in the form of an impact shock wave. The parameters that define the shock wave are the reflected pressure and the duration of the positive phase. The time integral of the reflected pressure over the duration of the positive phase is known as the reflected impulse. Public buildings, such as railway stations, embassies and airports, should be designed to ensure as much safety of the occupants as possible. Furthermore, counter-measures need to be taken to reduce the severity of the explosion; indirect means such as using blast barriers to protect important infrastructures and people inside them are widely used [3] [4] [5]. Therefore, there is an urgent need to directly enhance the blast resistance of important structures by using new structural types or new materials.

Newly developed mobile and lightweight materials such as aluminum foam are very attractive for use as protective layers in many applications because they have lightweight, are cheaper, and have greater energy absorption capacities than traditional technologies [6] [7] [8] [9] [10].

The metallic foam consists of a matrix of aluminum filled with pockets of air. Because of its long, plastic plateau in compression, metallic foam allows high energy absorption at a nearly constant stress level, making it an ideal material for mitigating the effects of explosive loads on a structural system [11] [12].

Metallic sandwich structures are widely used in various fields, such as aerospace, marine and railway systems because using metallic structures provides low density, high strength and good energy absorbing capability [13] [14]. When an explosion occurs near a foam-cladded reinforced concrete member, the foam layer compresses and absorbs a large amount of energy and offers protection for the members against blast loads [15].

Another means of protecting important structures against the intensive pressure of the explosions which causes critical damage to the nearby buildings and human beings in the perimeter of the explosion [4] [16] [17] is using different sizes and shapes of Barriers to diffract the blast wave, leaving behind it a complex flow field that changes the load exerted on the target [9] [10] [18] [19]. Numerous researchers have studied the effects of shock waves on different geometric configurations theoretically, numerically and experimentally [20]-[27].

Ordinary concrete, which is one of the most widely used construction materials, is well-known to be unsuitable to be used for protection against extreme loading such as blast loading because of its poor energy absorption capacity, poor tensile strength and brittle nature. Several methods have been introduced by many researchers, including the addition of discontinuous fibers [28] [29] [30], the use of continuous textile reinforcements to overcome the drawbacks of ordinary concrete [31] [32].

Although high-strength concrete (HSC) and high-performance concrete (HPC) are generally used in military and civil constructions to withstand blast and impact loads, they still lack sufficient strength under a high loading rate. Therefore, there is a growing demand for new construction materials with superior performance to withstand such extreme loading conditions.

Ultra-high performance concrete (UHPC) is a promising construction newly developed material that contains fibers, a low water-binder ratio and a high micro-silica content with the replacement of coarse aggregate with fine aggregate [33]. Compared with conventional concretes, UHPC is known for its outstanding strength, toughness, durability, ductility, serviceability and safety [34] [35] [36] [37] [38], so these characteristics enable it to withstand high-strain loads such as impact and blast loading.

When an explosion is in close range or contact with a concrete structure, the surface facing the detonation experiences compression and may fail under high compressive force and generate cratering. While the distant face experiences tensile forces when the compressive shock wave propagates in the structure and interacts with the free surface, it reflects and converts to a tensile wave. Due to the low tensile resistance of concrete, if the net stress exceeds concrete dynamic tensile strength cracks will be formed. Furthermore, if the trapped impulse is large enough to overcome the resistant forces such as the bond, and shear around the perimeter of the cracked portion, the cracked-off parts will displace from the backside of the structure.

When a single isolated building is loaded by the blast wave produced by the detonation of a quantity of high explosives, calculation of the pressure–time history experienced by the building is generally relatively straightforward, particularly for the side of the building directly facing the blast. However, if the geometry of the scenario becomes more complex (e.g. when an explosive device is detonated in an urban environment where there are many buildings), assessment of the loading experienced by a particular building becomes more difficult. Such assessment becomes even more complicated should the facades of some buildings partly or completely fail, allowing the blast to enter the building.

This paper aims to explain the different properties of the explosion process and summarize the different approaches to predict the different effects of blast loads especially on structures and also illustrate the response of structures to these loads.

2. Explosion and Blast Phenomenon

2.1. Explosion

Explosion is defined as a very rapid release of a large amount of energy within a limited space [39]. An explosion is typically categorized as a nuclear, physical or chemical event. Eruptions of a volcano, catastrophic failure of pressure vessels or violent mixing of liquids at different temperatures are considered physical explosions. The energy released from the formation of different atomic nuclei

during the redistribution of protons and neutrons within different interacting atomic nuclei forms an explosion. Most practical explosives in a solid or liquid state are also known as condensed explosives [39].

When an explosion initiates in air the following sequence of events happens [39] [40]:

- High temperature and pressure are released from the center of explosion.
- Gas expands violently and high pressure released pushes surrounding air out of the volume that it occupies.
- Most of the energy released by the explosive is transmitted to the air pushed out (now in a compressed state) and forms a blast wave in front of the gas from the explosive reaction.
- The blast wave moves outward from the source of explosion and air pressure at the blast wave decays with distance.
- The air pressure drops and falls below atmospheric pressure before it return to a state of equilibrium where there is no gas or air being pushed away from the source.

2.2. Blast Loads

Blast loads can be classified into confined and unconfined explosions. Confined explosions occur when the blast initiates inside a structure and the shock load initiated from the explosion is amplified with reflections of the internal surfaces. When the explosive is detonated in an open source and the blast waves propagate away from the source towards the structure, this is considered an unconfined explosion. Unconfined explosions can be classified into three types: free air burst explosions, air burst explosions, and surface burst explosions. This classification is based on their locations relative to the surrounding surfaces [41].

Calculating TNT equivalence, written as (W_{TNTeq}), is the first step in the quantification of blast waves. When determining the blast wave parameters generated by an explosive other than TNT, the initial step is to convert the mass of the explosive to an equivalent mass of TNT. For calculating the equivalent mass of TNT (W_{TNTeq}, the mass of the explosive (W_e) is scaled by a conversion factor that is based on its specific energy (Q_e) and the specific energy of TNT(Q_{TNT}) [40]:

$$W_{TNTeq} = \left(Q_e / Q_{TNT}\right) W_e \tag{1.1}$$

A list of conventional explosives used in military and commercial applications can be seen in **Table 1**, along with values for mass specific energy and the TNT equivalent.

2.3. Prediction of Blast Parameters

The parameters of the blast wave in a free air burst explosion are important for characterizing the loads that will be used to design a structure. **Figure 1** illustrates the free air burst wave front. Numerical analysis by Brode [43] produced the relationships (*i.e.* Equations (1.2) and (1.3)) between peak side-on overpressure, P_{so} and scaled distance Z.

Table 1. Conversion factor for explosives [42].

Explosive	Mass Specific Energy Q_e (kJ/kg)	TNT Equivalent (Q_e/Q_{TNT})
TNT	4520	1.00
C4	-	1.19 - 1.37
Nitroglycerin dynamite	2710	0.60
Comp-B	5190	1.15
Semtex	5660	1.25
RDX	5360	1.19
ANFO	3930	0.87

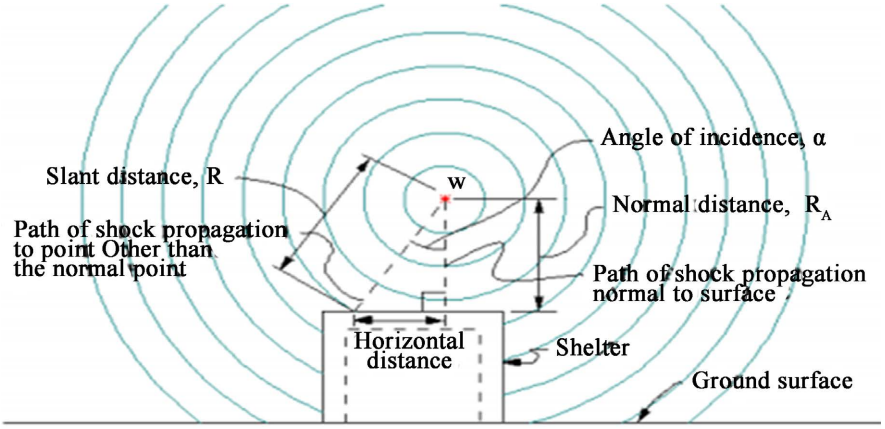

Figure 1. Free air burst wave front [44].

$$P_{so} = \frac{6.7}{Z^3} + 1 \quad (P_{so} > 10 \text{ bar}) \tag{1.2}$$

$$P_{so} = \frac{0.975}{Z^3} + \frac{1.445}{Z^3} + \frac{5.85}{Z^3} - 0.019 \quad (0.1 \text{ bar} < P_{so} < 10 \text{ bar}) \tag{1.3}$$

The scaled distance (Z) is given by:

$$Z = \frac{R_c}{W^{1/3}} \tag{1.4}$$

where, R_c is the distance from the center of the charge (spherical) and W is the TNT equivalent charge weight ($W_{TNT_{eq}}$) defined by Equation (1.1).

Newmark and Hansen [45] introduced Equation (1.5) to calculate the maximum blast pressure (P_{so}), in bars, for a high explosive charge detonates at the ground surface as:

$$P_{so} = 6784\frac{W}{R^3} + 93\left(\frac{W}{R^3}\right)^{\frac{1}{2}} \tag{1.5}$$

Another expression of the peak overpressure in KPa was introduced by Mills [46], given in Equation (1.6), in which (W) is expressed as the equivalent charge weight in kilograms of TNT, and Z is the scaled distance:

$$P_{so} = \frac{1772}{Z^3} - \frac{114}{Z^2} + \frac{108}{Z} \tag{1.6}$$

A typical pressure-time history plot for a blast wave in air is shown in Figure 2. At the time of arrival (t_a), the rise from ambient pressure (P_o) to the incident overpressure (P_{so}) is assumed to be instantaneous. The pressure decays to a minimum under pressure (P_s^-) before returning ambient conditions. The duration of the positive phase (t_p) occurs in the time span where the pressure remains greater than ambient. The pressure remains decaying until it falls below ambient pressure, during the negative phase duration (t_n). The exponential pressure decay was described using the Friedlander equation [39] [40], as:

$$P(t) = P_{so}\left(1 - \frac{t}{t_0}\right)e^{-\left(\frac{bt}{t_0}\right)} \tag{1.7}$$

where b is the waveform parameter.

Another parameter important to the analysis of blast waves is specific impulse (i_s), which is the area under the positive phase of the pressure-time curve and this is defined using:

$$i_s = \int_{t_a}^{t_p} P_{so}(t)\,\mathrm{d}t \tag{1.8}$$

For simplified analysis, the decay may be approximated as linear from t_a to t_p the impulse may be written as:

$$i_s = \frac{1}{2} t_p P_{so} \tag{1.9}$$

The duration of the blast wave profile when the pressure dips below than ambient pressure is called the negative phase. According to Brode [40], the minimum under pressure, P_{so}^-, of the negative phase can be determined utilizing:

$$P_{so}^- = -\frac{0.35}{Z}(\text{bar}) \tag{1.10}$$

where the pressure is in bar and the scaled distance is greater than 1.6. The impulse of the negative phase is denoted i^- and can be calculated using:

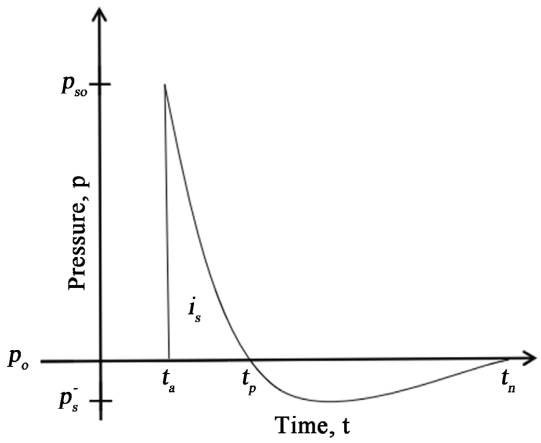

Figure 2. Pressure-time history for blast wave in free air [47].

$$i^{-} \approx i_s\left[1-\frac{1}{2Z}\right] \tag{1.11}$$

The parameters of the negative phase are often unimportant in the design of structural components because the positive phase pressures and impulses for threats of interest are significantly higher and have a more significant effect on the structure response. Other important parameters of the blast wave are the shock front velocity (U) the wave length of the positive phase (L_w), reflected pressure (P_r), and reflected impulse (i_r).

Graphical methods are convenient for determining the blast wave parameters described above. Several references such as TM-5 [44], provide plots of the different parameters for a free air burst (Y-axis) versus the scaled distance (X-axis) as plotted in **Figure 3**, where this figure can be used to determine the different blast wave parameters in the free air during the positive phase only using the scaled distance.

The magnitude of the reflected pressure (P_r) and impulse (i_r) will be greater than the over peak pressure and impulse. This enhancement occurs because in addition to the potential energy stored as a pressure differential in the blast wave, the air particles that comprise the blast wave have velocity and thus, kinetic energy. In the case when the wave encounters an infinitely large rigid wall wherein the particles are brought to rest and are compressed at the surface resulting in an increase in pressure [47]. An idealized pressure-time history on a

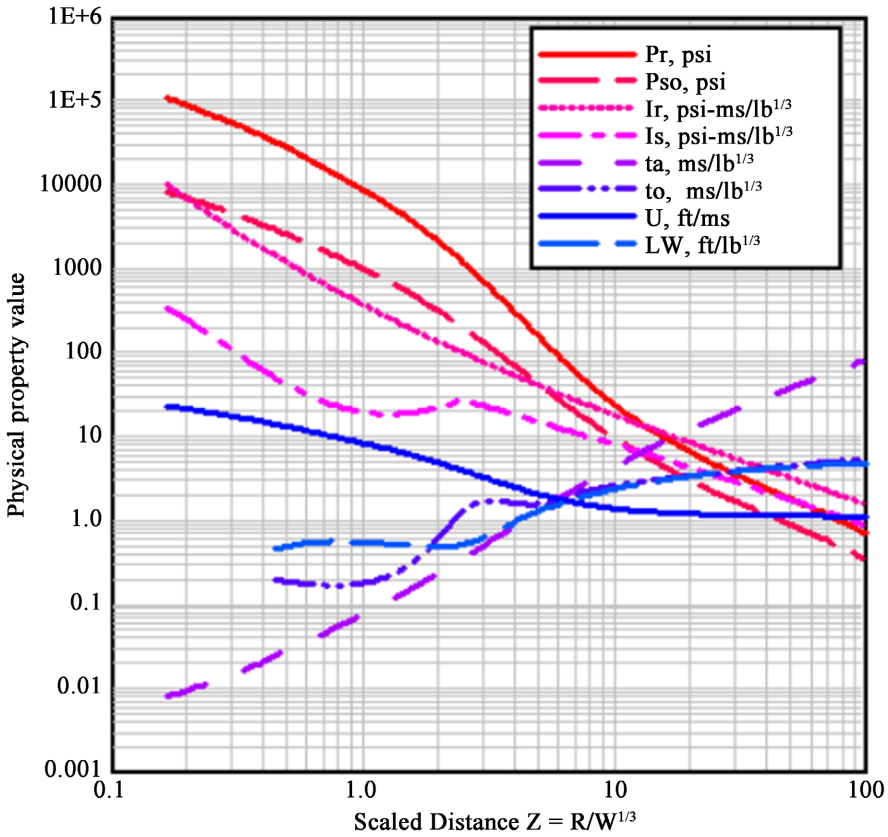

Figure 3. Positive phase free air burst blast wave parameters vs. scaled distance [44].

structure is shown in Figure 4, denoting the incident overpressure (P_s) and the reflected blast wave overpressure (P_r).

When the angle of incidence is zero the peak reflected pressure (P_r) can be calculated by the Rankine-Hugoniot prediction [39] using:

$$P_r = 2P_{so} + (\gamma + 1)q_s \tag{1.12}$$

where, γ is the specific heat ratio of a real gas and q_s is the dynamic pressure which can be determined using:

$$q_s = \frac{1}{2}\rho_s u_s^2 \tag{1.13}$$

where, ρ_s is the density of the air, and u_s is the particle velocity behind the wave front. The particle velocity (u_s) can be computed utilizing:

$$u_s = \frac{a_o P_s}{\gamma P_o}\left[1 + \left[\frac{\gamma + 1}{2\gamma}\right]\frac{P_s}{P_o}\right]^{\frac{1}{2}} \tag{1.14}$$

where, a_o is the speed of sound at ambient conditions. Substitutions of Equations (1.12) and (1.13) into (1.14) gives:

$$P_r = 2P_s\left[\frac{7P_o + 4P_s}{7P_o + P_s}\right] \tag{1.15}$$

When $\gamma = 1.4$ for air. The reflected pressure will be twice the incident side-on pressure for the case when P_s is small relative to P_o ; which arises when the explosion is small and at long range. The reflected pulse can be as much as eight times the incident side-on pressure for the case when the P_s is large compared to P_o which arises when the charge is large and close in. It should be noted that these equations are only applicable when Z is greater than 0.134 ft/lb$^{1/3}$ (0.053 m/kg$^{1/3}$) which represents the radius of a spherical TNT explosive and the surface of the explosive [39].

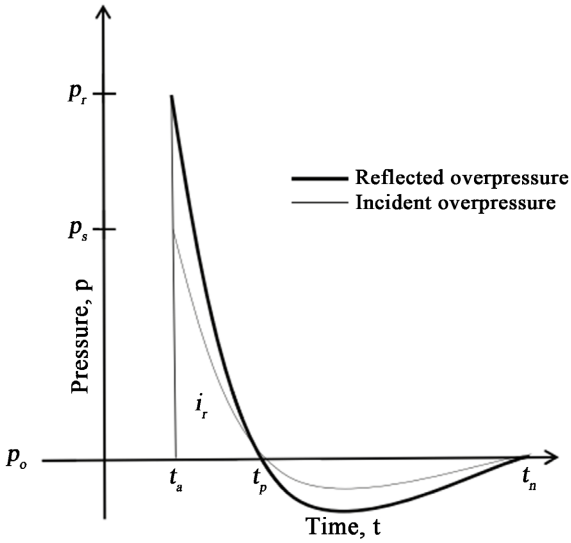

Figure 4. Pressure-time history of reflected airburst [47].

2.4. Methods for Prediction of Blast Effects

The following methods are available for prediction of blast effects on building structures:

1) Empirical methods are related to experimental data. Most of these approaches are limited by the extent of the underlying experimental database. The accuracy of all empirical equations diminishes as the explosive event becomes increasingly near field [48].

2) Semi-empirical methods are based on simplified models of physical phenomena. The attempt is to model the underlying important physical processes in a simplified way. These methods depend on more extensive data and case study than that of empirical methods. Thus, the predictive accuracy is generally better than that provided by the empirical methods [48].

3) Numerical (or first-principle) methods are based on mathematical equations that describe the basic laws of physics governing a problem. These principles include conservation of mass, momentum, and energy. In addition, the physical behavior of material is described by constitutive relationships. These models are commonly termed computational fluid dynamics (CFD) models [48].

There are other attempts to predict the blast effects, among them, Khadid [49] who studied the fully fixed stiffened plates under the effect of blast loads to determine the dynamic response of plates with different stiffener configurations. This study included the effect of mesh density, time duration and strain rate sensitivity. The author used the finite element method and the central difference method for the time integration of the nonlinear equations of motion to obtain numerical solutions.

Blance *et al.* [50] presented an empirical approach for the external blast load on structures. The authors used models based on TM5-1300 in pure Lagrange approach for blast evaluation leads to more precise and conservation load.

Pandey [51] studied the effects of an external explosion on the outer reinforced concrete shell of a typical nuclear containment structure. The analysis was performed using non-linear material models till the ultimate stages. An analytical procedure for nonlinear analysis by adopting the used model was implemented into a finite element code DYNAIB.

Ngo *et al.* [52] gave an overview on the analysis and design of structures subjected to blast loads for understanding the blast loads and dynamic response of various structural elements.

3. Air-Blast Modeling

The shock of the blast wave is generated when the surrounding atmosphere is subject to an extreme compressive pulse generated outward from the center of the explosion. Transient pressure greater than ambient pressure is defined as overpressure. The peak overpressure Ps+ is the maximum value of the overpressure at a given location [53].

3.1. Blast Scaling Law

Characteristics of the blast wave generated in an explosion depend on both the explosive energy release and the nature of the medium through which the blast propagates. These characteristics are measured under controlled conditions in experiments (providing a reference set of explosion data) that can be used to obtain data on other explosions using scaling laws. The most common form of blast scaling is Hopkison according to ref. [39] or cube root scaling law. This law states that when two charges of the same explosive and geometry, but of different size are detonated in the same atmosphere, the shock waves produced are similar in nature at the same scaled distances. The scaled distance Z, is defined as:

$$Z = \frac{R}{\sqrt[3]{W}}, \mathrm{m/kg^{-1/3}} \tag{1.16}$$

where R is the distance from the center of the explosion to a given location and W is the weight of the explosive. In addition to this, the explosive yield factor λ, is useful in blast scaling. This is defined as:

$$\lambda = \sqrt[3]{\frac{W}{W_r}} \tag{1.17}$$

where W_r is the weight of the reference explosion. Thus similar shock effects are seen at similar scaled distances:

$$Z = \frac{R}{\sqrt[3]{W}} = \frac{R_r}{\sqrt[3]{W_r}} \tag{1.18}$$

where R_r is the distance of the reference explosion, and is related to R through:

$$R = \lambda R_r \tag{1.19}$$

Scaling can be applied to time parameters. The scaled time τ_{sc} for a time t is defined as:

$$\tau_{sc} = \frac{t}{\sqrt[3]{W}} \tag{1.20}$$

3.2. Blast Wave Reflections

When a blast wave strikes a surface, which is not parallel to its direction of propagation, a reflection of the blast wave takes place. The reflection can be either normal reflection or an oblique reflection. There are two types of oblique reflection, either regular or Mach reflection; the type of reflection depends on the incident angle and shock strength [53] [54].

3.2.1. Normal Reflection

A normal reflection takes place when the blast wave hits perpendicular to a surface, as shown in **Figure 5**. The medium has a particle velocity, U_x, before the incident shock wave, U_s, passes the medium.

After passage, the particle velocity increases to U_P. Furthermore, the overpressure

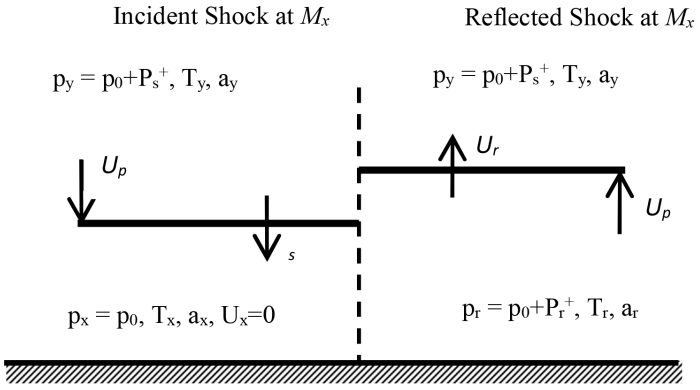

Figure 5. Normal reflection in air from a rigid wall [54].

increases from P_x to P_y (P_x refers usually to atmospheric overpressure), the temperature increases from T_x to T_y and the sonic speed increases from α_x to α_y (α_x is approximately 340 m/s in air).

When the blast wave hits a rigid surface, the direction will be shifted rapidly, and, as a consequence, the particles at the surface possess a velocity relative to those further from the surface that are still in motion. This relative velocity is equal in magnitude and opposite in direction to the original particle velocity and gives the effect of a new shock front moving back through the air; the reflected shock, U_r. However, since the air conditions have changed, the reflected shock will have different properties. The reflected overpressure increases to P_r, temperature increases to T_r and sonic speed will be α_r.

For shock waves it is common to describe the velocity as a Mach number, which is defined as the actual velocity (of the shock front) in the medium divided by the sonic speed of the undisturbed medium. For example, the shock front will have a velocity with a Mach number M_r into air that had a velocity with M_x at the incident shock. The properties of the reflected blast wave can be described in terms of a reflection coefficient, defined as the ratio of reflected overpressure to the overpressure in the incident blast wave. It can be shown that for an ideal gas with a specific gas constant ratio of 1.4, the reflection coefficient C_r is, according to ref. [55].

$$C_r = \frac{P_r - P_x}{P_y - P_x} = \frac{8M_x + 4}{M_x + 5} \tag{1.21}$$

From Equation (1.21), it can be seen that for a shock front moving with M_x equal to one, *i.e.* at sonic speed, the reflection coefficient will be two. This means that the overpressure is twice in the reflected blast wave. With increasing speed for the shock front, M_x, the reflection coefficient approaches eight. However, that is for ideal gas with a specific gas constant ratio of 1.4. In a real blast wave, the specific gas constant ratio is not constant, and the coefficient is pressure-dependent; the reflection coefficient increases with increasing pressure.

3.2.2. Regular Reflection

In a regular reflection the blast wave has an incident shock at M_x with an angle

of β and reflection takes place. The reflected shock at M_r has an angle of δ as shown in Figure 6. The angle of reflection is not generally equal to the angle of incidence. The air conditions in front of the incident shock (region 1) are still at pressure P_x and temperature T_x. Behind the incident shock (region 2), the air conditions are the same as for free air shock, with pressure P_y and temperature T_y. The air conditions from the reflected shock (region 3), have the pressure P_r and temperature T_r.

3.2.3. Mach Stem Formation

There is a critical angle that depends on the shock strength, where an oblique reflection cannot occur. According to Baker [54], Ernst Mach showed that the incident shock and the reflected shock coalesce to form a third shock front. The created shock front is termed the Mach stem or Mach front, which is moving approximately parallel to the ground surface, as shown in Figure 7, with increasing height of the shock front. The point where the three shock fronts meets is termed the triple point.

3.3. Prediction of Blast Wave Characteristics

3.3.1. Peak Overpressure Prediction

The most destructive effect of a blast wave is generally characterized by the peak overpressure. The magnitude of the peak overpressures is a function primarily of the weapon yield, the height of burst, and the distance from the burst. There are several sets of overpressure equations developed using both numerical and experimental techniques [56]. The Brode equations are:

$$P_s = \frac{670}{Z^3} + 100\left[\text{KPa}\right] \quad \text{for} \quad P_s > 1000 \text{ KPa} \tag{1.22}$$

$$P_s = \frac{97.5}{Z} + \frac{145.5}{Z^2} + \frac{585}{Z^3} - 1.9\left[\text{KPa}\right] \quad \text{for} \quad 10 < P_s < 1000 \text{ KPa} \tag{1.23}$$

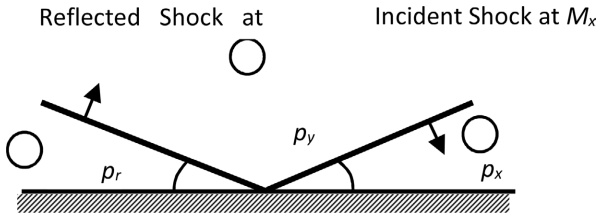

Figure 6. Oblique reflection [54].

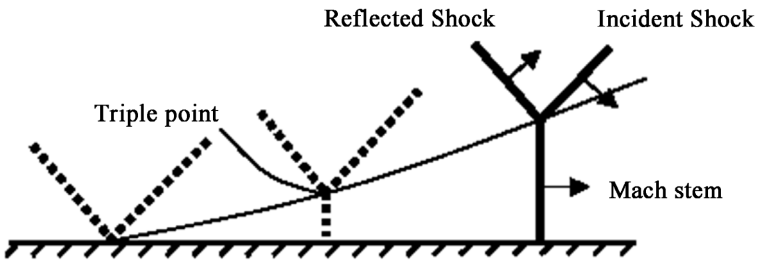

Figure 7. Mach stem formation [8].

The equations presented by Henrych divide the analysis into three fields, a near middle and far field:

$$P_s = \frac{1407.2}{Z} + \frac{554}{Z^2} - \frac{35.7}{Z^3} + \frac{0.625}{Z^4} \left[\text{KPa}\right] \quad (\text{for} \quad 5 < Z < 30) \tag{1.24}$$

$$P_s = \frac{619.4}{Z} - \frac{32.6}{Z^2} - \frac{213.2}{Z^3} \left[\text{KPa}\right] \quad (\text{for} \quad 30 < Z < 100) \tag{1.25}$$

$$P_s = \frac{66.2}{Z} + \frac{405}{Z^2} + \frac{328.8}{Z^3} \left[\text{KPa}\right] \quad (\text{for} \quad 100 < Z < 1000) \tag{1.26}$$

where Z is the scaled distance and is determined from Equation (1.16).

The Brode equations give good correspondence to experimental peak overpressure results in the middle and far field, but not in the near field. The Henrych equations give good correspondence in the near and far fields, but not in the middle field.

The peak overpressure P_s (in *psi*) of nuclear explosion, according to [57] given:

$$P_s(r,z) = \frac{10.47}{r^{a(z)}} + \frac{b(z)}{r^{c(z)}} + \frac{d(z)\cdot e(z)}{1 + f(z) r^{g(z)}} + h(z,r,y) \tag{1.27}$$

where:

$$a(z) = 1.22 - \frac{3.908 z^2}{1 + 810.2 z^5}$$

$$b(z) = 2.321 + \frac{6.195 z^{18}}{1 + 1.113 z^{18}} - \frac{0.03831 z^{17}}{1 + 0.02415 z^{17}} + \frac{0.6692}{1 + 4164 z^8}$$

$$c(z) = 4.153 - \frac{1.149 z^{18}}{1 + 1.641 z^{18}} - \frac{1.1}{1 + 2.771 z^{2.5}}$$

$$d(z) = -4.166 + \frac{25.76 z^{1.75}}{1 + 1.382 z^{18}} + \frac{8.257 z}{1 + 3.219 z}$$

$$e(z) = 1 - \frac{0.004642 z^{18}}{1 + 0.003886 z^{18}}$$

$$f(z) = 0.6096 + \frac{2.879 z^{9.25}}{1 + 2.359 z^{14.5}} - \frac{17.15 z^2}{1 + 71.66 z^3}$$

$$g(z) = 1.83 + \frac{5.361 z^2}{1 + 0.3139 z^6}$$

and

$$h(z,r,y) = \frac{-\left(64.67 z^5 + 0.2905\right)}{1 + 441.5 z^5} - \frac{1.389 z}{1 + 49.03 z^5} + \frac{8.808 z^{1.5}}{1 + 154.5 z^{3.5}} + \frac{0.0014 r^2}{\left(1 - 0.158 r + 0.0486 r^{1.5} + 0.00128 r^2 (1 + 2y)\right)}$$

where x is the scaled ground range, and y is the scaled height of burst, $r = \sqrt{x^2 + y^2}$ in kft/kt$^{1/3}$ and $z = y/x$.

If x, y and r are in km/kt$^{1/3}$, the peak overpressure P_s (in kPa) is

$$P_s(r,z)=\beta\left[\frac{10.47}{(\alpha r)^{a(z)}}+\frac{b(z)}{(\alpha r)^{c(z)}}+\frac{d(z)\cdot e(z)}{1+f(z)(\alpha r)^{g(z)}}+h(z,r,y)\right],\text{kPa} \quad (1.28)$$

In which

$$h(z,r,y)=\frac{-\left(64.67z^5+0.2905\right)}{1+441.5z^5}-\frac{1.389z}{1+49.03z^5}+\frac{8.808z^{1.5}}{1+154.5z^{3.5}}+\frac{0.0014(\alpha r)^2}{\left(1-0.158(\alpha r)+0.0486(\alpha r)^{1.5}+0.00128(\alpha r)^2(1+2y)\right.}$$

$\alpha=(0.3048)^{-1}$, (kft - km), $\beta=(100/14.504)$, (kPa).

The above expressions are appropriate for calculation of peak overpressures over a range from 1 to 10,000 psi (7 kPa to 70 MPa), and for a reference weapon yield (1 kt or 1 Mt), and can be determined for other yields by scaling law.

The duration of the positive phase, t_0, is a function the total energy yield of the explosion. Typical value of t_0 for high explosives can be found from [58].

$$\frac{t_0}{W^{1/2}}=\frac{980\left(1+(z/0.54)^{10}\right)}{\left[1+(z/0.02)^3\right]\left[1+(z/0.74)^6\right]\left[1+(z/6.9)^2\right]^{1/2}} \quad (1.29)$$

where t_0 in milliseconds and z in m/kg$^{1/3}$.

For nuclear explosions:

$$\frac{t_0}{W^{1/3}}=\frac{180\left(1+(z/100)^3\right)^{1/2}}{\left[1+(z/40)^{1/2}\right]\left[1+(z/285)^5\right]\left[1+(z/50000)^2\right]^{1/6}} \quad (1.30)$$

where t_0 in seconds and z in m/kt$^{1/3}$.

3.3.2. Dynamic Overpressure Prediction

In many cases, depending on the structure geometry's, the strong transient winds behind the shock front can be of greater significance. These drag forces are a function of the size and shape of the structure [55] and the peak value of the dynamic pressure resulted from the wind behind the shock front. To predict the peak value of dynamic pressure, several wave-front parameters are needed. These were first identified by Rankine and Hugoniot in 1870 [55] and include P_s, peak overpressure; ρ_s, static density; and u_s, the blast wave front velocity. There are two possible approaches to determining these parameters: the use of a set of pre-computed blast curves, Or the use of a set of equations for normal reflections given P_s:

$$u_s=\frac{C_0P_s}{\gamma_hP_0}\left[1+\left(\frac{\gamma_h+1}{2\gamma_h}\right)\frac{P_s}{P_0}\right]^{-1/2} \quad (1.31)$$

$$\rho_s=\rho_0\left[\frac{(\gamma_h+1)P_s+2\gamma_hP_0}{(\gamma_h-1)P_s+2\gamma_hP_0}\right] \quad (1.32)$$

where C_o is the sound speed, P_o is the ambient pressure, ρ_0 is the density of air and γ_h is the ratio of specific heat of air.

The peak dynamic pressure, P_d, is then defined as:

$$P_d = \frac{1}{2}\rho_s u_s^2 \tag{1.33}$$

The arrival time of dynamic pressure is considered to be the same as that of the peak overpressure. The dynamic pressure positive phase duration, t_d, is expressed in seconds for 1 megaton surface nuclear burst as:

$$t_d = \left[\frac{4}{1+0.085P_s+0.0075P_s^2} + \frac{0.077P_s}{1+0.00042P_s^2} + \frac{0.02662P_s}{1+0.011P_s}\right] W^{1/3} \tag{1.34}$$

In which W is the explosion yield in megatons. Values for other yields can be obtained by the scaling law.

3.3.3. Reflected Overpressure Prediction

The ratio of reflected to incident overpressures is called the reflection factor, which is a function of the peak overpressure in the incident wave and the angle at which the wave strikes the surfaces. When the blast reaches an object at right angles, or nearly so, the resulting reflection produces a peak-reflected overpressure, P_r, given by [57] [59] [60]:

$$P_r = 2P_s + (1+\gamma_h)P_d \tag{1.35}$$

Considering the ideal gas conditions (γ_h = 1.4) and substituting for P_d from Equation (1.33), the peak reflected overpressure is expressed as:

$$\frac{P_r}{P_s} = 2 + \frac{6P_s}{P_s+7P_0} \tag{1.36}$$

Equation (1.35) is valid for ideal gas when the overpressure, P_s, is less than 10 bars. The peak reflected overpressure can approach a value of twice the peak incident overpressure for weak shocks in which the peak dynamic pressure is negligible, but may approach a value of eight times the peak overpressure for strong shocks in which the peak dynamic pressure is dominant [53].

It is suggested [53] that one can roughly estimate the reflected impulse, i_r, if the side-on impulse is known, by assuming similarity between the time histories of side-on overpressure and normally reflected overpressure. This assumption gives:

$$\frac{i_r}{i_s} = \frac{P_r}{P_s} \tag{1.37}$$

The actual positive duration is replaced by a function duration expressed as:

$$t_r = 2i_r / P_r \tag{1.38}$$

4. Structural Responses to Blast Loading

Studying the response of blast-loaded structures involves the effect of non-linear inelastic material behavior, high strain rates and the time-dependent deformations. Such study is very complicated in analyzing the dynamic response of a

structure [48].

Therefore, to simplify the analysis, a number of assumptions related to the response of structures and the loads were assumed [48]. A structure is idealized as a single degree of freedom (SDOF) system to achieve the principles of this analysis [61]. The elastic SDOF systems and the elasto-plastic SDOF systems are presented in the following subsections.

4.1. Elastic SDOF System

The simplest discretization of transient problem is achieved by using of the SDOF approach. The actual structure is replaced by an equivalent system of one concentrated mass and one weightless spring representing the resistance of the structure against deformation [48]. **Figure 8** illustrates the idealized spring mass system. The structural mass (M) is under the effect of an external force ($F(t)$) and the structural resistance(R_m) is expressed in terms of the vertical displacement (y) and the spring constant (k).

The blast load can be represented as a triangular pulse having a peak force (F_m) and positive phase duration (t_d). The forcing function can be identified as:

$$F(t) = F_m\left(1-\frac{t}{t_o}\right) \tag{1.39}$$

The blast impulse is defined as the area under the force-time curve, and is given by:

$$i = \frac{1}{2}F_m t_d \tag{1.40}$$

The equation of motion of the un-damped elastic SDOF system for a time ranging from zero to positive phase duration (t_d), is given by Biggs [62] as:

$$M\ddot{y} + Ky = F_m\left(1-\frac{t}{t_o}\right) \tag{1.41}$$

where, $\ddot{y}$ is the acceleration.

Solving this equation of motion, the general solution can be expressed as:

$$y(t) = \frac{F_m}{K}(1-\cos\omega t) + \frac{F_m}{Kt_d}\left(\frac{\sin\omega t}{\omega} - t\right) \tag{1.42}$$

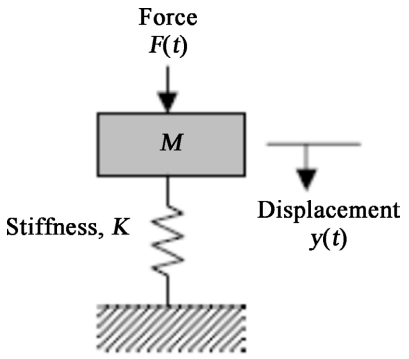

Figure 8. Idealized SDOF system.

$$\dot{y}(t) = \frac{F_m}{K}\left[\omega \sin \omega t + \frac{1}{t_d}(\cos \omega t - 1)\right] \tag{1.43}$$

where, *y(t)* is the displacement function, while $\dot{y}(t)$ is the velocity function.

The natural circular frequency of vibration of a structure (ω) can be calculated as:

$$\omega = \frac{2\pi}{T} = \sqrt{\frac{K}{M}} \tag{1.44}$$

where, T is the natural period of vibration of a structure.

The maximum response is defined as the maximum dynamic deflection ($Y_{\max}$) which occurs at time tm. This deflection can be evaluated by setting $\dot{y}(t)$ in Equation (1.43) equals to zero, when the structural velocity is zero. The dynamic load factor (DLF) is defined as the ratio of the maximum dynamic deflection ($Y_{\max}$) to the static deflection (Y_{st}) resulted from the static application of the peak load (F_m) [48] and it is defined by:

$$\text{DLF} = \frac{Y_{\max}}{Y_{st}} = \frac{Y_{\max}}{F_m/K} = \psi(\omega t_d) = \psi\left(\frac{t_d}{T}\right) \tag{1.45}$$

4.2. Elasto-Plastic SDOF System

Structural elements are expected to experience large inelastic deformation under blast load or high velocity impact [48]. Exact analysis of dynamic response is then only possible using step-by-step numerical analysis requiring nonlinear dynamic finite-element software.

The maximum displacement is presented in chart form TM 5-1300 [44], as a family of curves for selected values of R_u/F_m showing the required ductility μ as a function of t_d/T in which R_u is the ultimate or maximum resistance of the structure and T is the natural period. The maximum response of elasto-plastic SDOF system subjected to a triangular load is shown in **Figure 9**.

5. Materials Behavior at High Strain Rate

Blast loads ideally produce very high strain rate in the range of 10^2 - 10^4 s^{-1}. This rate would change the dynamic mechanical properties of target structures and, accordingly, the speculated damage mechanisms for different structural elements. For reinforced concrete structures subjected to blast effects, the strength of concrete and steel reinforcing bars can be increased significantly due to strain rate effects. The approximate ranges of the expected strain rates for different loading conditions [63] are shown in **Figure 10**. It can be observed that quasi-static (ordinary) strain rate is located in the range: 10^{-6} - 10^{-5} s^{-1}, while blast loads are associated with strain rates ranging from 10^2 - 10^4 s^{-1}. The dynamic properties and the behavior of concrete and steel reinforcing bars are described in the following subsections.

5.1. Dynamic Properties of Concrete at High Strain Rates

The mechanical properties of concrete subjected to dynamic loading are quite

different from those due to static loading. While dynamic stiffness does not vary a lot from the static stiffness, the stresses that are preserved for a certain period of time under dynamic conditions may gain values that are remarkably higher than the static compressive strength as shown in Figure 11 [52]. In compression

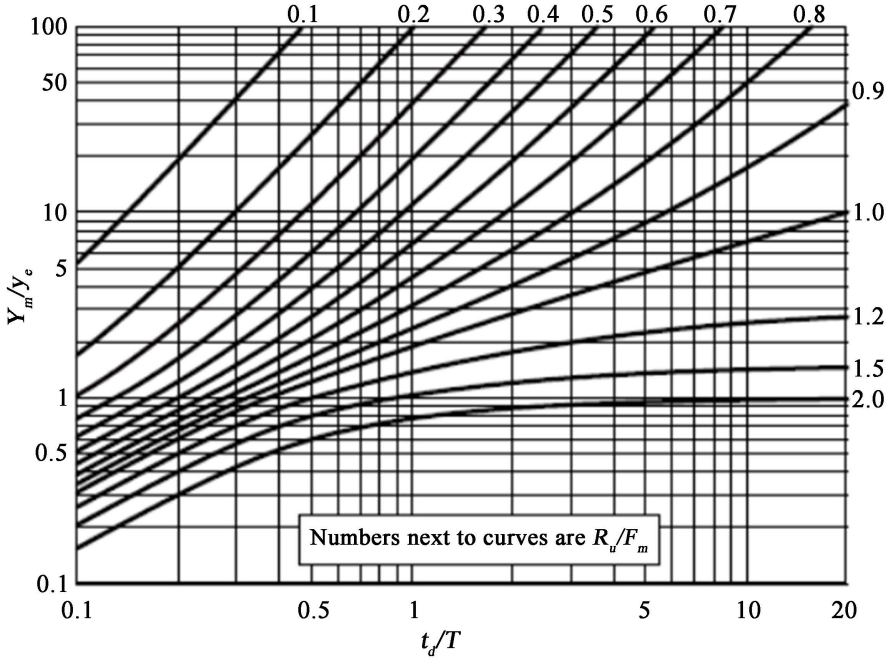

Figure 9. Maximum response of elasto-plastic SDOF system.

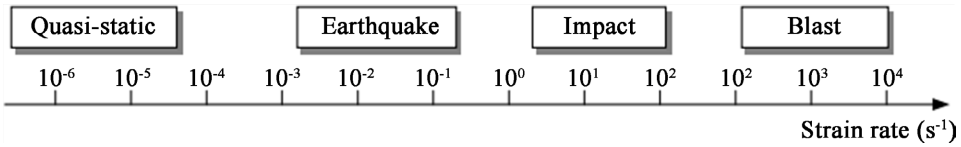

Figure 10. Strain rates associated with different types of loads [63].

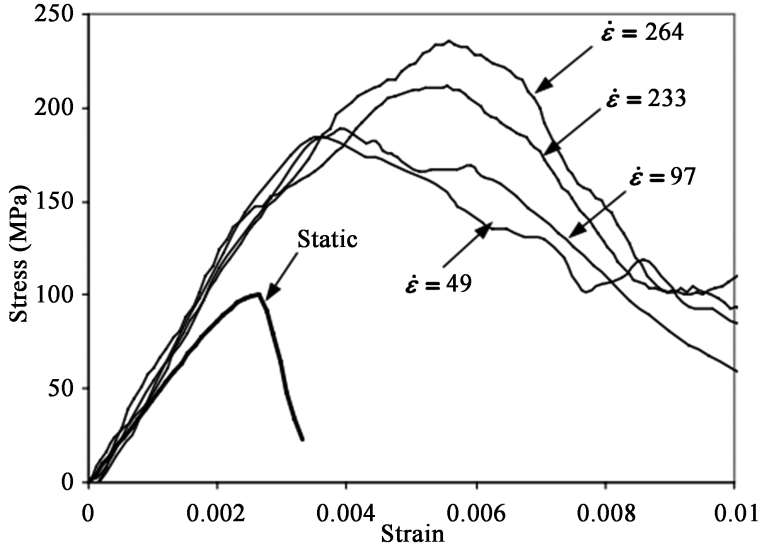

Figure 11. Stress-strain curves of concrete at different strain rates.

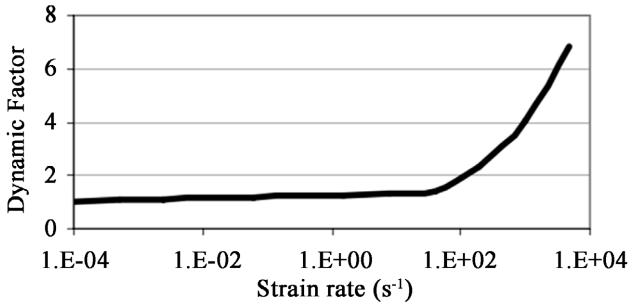

Figure 12. Dynamic increase factor for peak stress of concrete [63].

strength magnification factors as high as 4 in compression and up to 6 in tension for strain rates in the range: 102 - 103/sec have been observed [64].

For the increase in peak compressive stress (f_c'), a dynamic increase factor (DIF) is introduced in the Euro International Committee for Concrete- International Federation for Pre-stressing (CEB-FIP) model [65] as shown in **Figure 12** for strain-rate enhancement of concrete as follows:

$$\text{DIF} = \left(\frac{\dot{\varepsilon}}{\dot{\varepsilon}_s}\right)^{1.026\alpha} \quad \text{for } \dot{\varepsilon} \le 30\ \text{s}^{-1} \tag{1.46}$$

$$\text{DIF} = \gamma\left(\frac{\dot{\varepsilon}}{\dot{\varepsilon}_s}\right)^{1/3} \quad \text{for } \dot{\varepsilon} > 30\ \text{s}^{-1} \tag{1.47}$$

where, the strain rate is denoted by $\dot{\varepsilon}$ and the quasi-static strain rate $\dot{\varepsilon}_s$ equal 30×10^{-1} s^{-1}. Also the coefficients (γ) and (α) can be computed from:

$$\log \gamma = 6.156\alpha - 2 \tag{1.48}$$

$$\alpha = 1/\left(5 + 9\, f_c'/f_{co}\right) \tag{1.49}$$

where $f_{co} = 10$ MPa $= 1450$ psi .

5.2. Dynamic Properties of Reinforcing Steel at High Strain Rates

Metallic materials subjected to dynamic loading have an elastic and inelastic response that can easily be monitored and assessed due to their isotropic properties. Norris *et al.* [66] tested steel with two different static yield strengths of 330 and 278 MPa under tension at strain rates ranges of 10^{-5} to 0.1 s^{-1}. Strength increases of 9% - 21% and 10% - 23% were reported for the two steel types, respectively. Dowling and Harding [67] conducted tensile experiments using the tensile version of Split Hopkinton's Pressure Bar (SHPB) on mild steel using strain rates varying between 10^{-3} s^{-1} and 2000 s^{-1}. It was concluded from their experiments that materials of Body-Centered Cubic (BCC) structure, such as mild steel, showed the greatest strain rate sensitivity. It was also found that the lower yield strength of mild steel can almost be doubled; the ultimate tensile strength can be increased by about 50%; and the upper yield strength can be considerably higher. In contrast, the ultimate tensile strain decreases with increasing strain rate. Malvar [68] studied enhancing the strength of steel reinforcing bars under the effect of high strain rates. This was described in terms of the Dynamic In-

crease Factor (DIF), which can be evaluated for different steel grades and for yield stresses (f_y) ranging from 290 to 710 MPa as represented by Equation (1.48) [63].

$$\text{DIF} = \left(\frac{\dot{\varepsilon}}{10^{-4}} \right)^{\alpha} \tag{1.50}$$

where, for calculating yield stress $\alpha = \alpha_{fy}$ and

$$\alpha_{fy} = 0.074 - 0.04\left(f_y / 414 \right) \tag{1.51}$$

For ultimate stress calculation $\alpha = \alpha_{fu}$ and

$$\alpha_{fu} = 0.019 - 0.009\left(f_y / 414 \right) \tag{1.52}$$

6. Conclusion

The progressive development of military destructive weapons demands the improvement of the construction materials and techniques used in order to improve the blast resistance of fortified structures. Hence, protecting important structures against terroristic attacks is a very important topic as terrorist attacks have increased and developed a lot these days especially using blast loads. Therefore, this study is performed to cover the historical background and extensive literature review of the available previous research works focusing on the blast environment characteristics, fundamentals of blast loading and description of the methods used to predict blast loadings. Moreover, the research also covers a literature review on the response of structures subjected to blast loads and material behavior considering high strain rates. This is followed by exploring materials used to protect reinforced concrete structures subjected to blast loads. It is concluded that studying the blast phenomena, parameters, and methods of prediction is very important in order to design mitigation systems against explosion and blast loads for various types of applications.

Conflicts of Interest

The authors declare no conflicts of interest regarding the publication of this paper.

References

[1] Sandhu, I.S., Sharma, A., Singh, M.K., Kumari, R., Alegaonkar, P.S. and Saroha, D. (2017) Study of Blast Wave Pressure Modification through Rubber Foam. *Procedia Engineering*, **173**, 570-576. https://doi.org/10.1016/j.proeng.2016.12.099

[2] Wu, C. (2012) Research Development on Protection of Structures against Blast Loading at University of Adelaide. *Australian Journal of Structural Engineering*, **13**, 97-107.

[3] Hajek, R., Foglar, M. and Fladr, J. (2016) Influence of Barrier Material and Barrier Shape on Blast Wave Mitigation. *Construction and Building Materials*, **120**, 54-64. https://doi.org/10.1016/j.conbuildmat.2016.05.078

[4] Berger, S., Ben-Dor, G. and Sadot, O. (2015) Experimental and Numerical Investi-

gations of Shock-Wave Attenuation by Geometrical Means: A Single Barrier Configuration. *European Journal of Mechanics-B/Fluids*, **50**, 60-70. https://doi.org/10.1016/j.euromechflu.2014.11.006

[5] Éveillard, S., Lardjane, N., Vinçont, J.-Y. and Sochet, I. (2013) Towards a Fast-Running Method for Blast-Wave Mitigation by a Prismatic Blast Wall. *Comptes Rendus Mécanique*, **341**, 625-635. https://doi.org/10.1016/j.crme.2013.06.004

[6] Zhu, F., Zhao, L., Lu, G. and Wang, Z. (2008) Structural Response and Energy Absorption of Sandwich Panels with an Aluminium Foam Core under Blast Loading. *Advances in Structural Engineering*, **11**, 525-536. https://doi.org/10.1260/136943308786412005

[7] Li, S., Wang, Z., Wu, G., Zhao, L. and Li, X. (2014) Dynamic Response of Sandwich Spherical Shell with Graded Metallic Foam Cores Subjected to Blast Loading. *Composites Part A*: *Applied Science and Manufacturing*, **56**, 262-271. https://doi.org/10.1016/j.compositesa.2013.10.019

[8] Ismail, M.F., Jumahat, A., Abdullah, B., Hashim, U.R. and Aseri, S.E.A. (2015) Investigation on Energy Absorption of Aluminium Foam-CFRP Sandwich Panel Subjected to Impact Loading. *Jurnal Teknologi* (*Sciences & Engineering*), **75**, 113-116. https://doi.org/10.11113/jt.v75.5226

[9] Aghdamy, S., Wu, C. and Griffith, M. (2013) Simulation of Retrofitted Unreinforced Concrete Masonry Unit Walls under Blast Loading. *International Journal of Protective Structures*, **4**, 21-44. https://doi.org/10.1260/2041-4196.4.1.21

[10] Xia, Y., Wu, C., Zhang, F., Li, Z.-X. and Bennett, T. (2014) Numerical Analysis of foam-Protected RC Members under Blast Loads. *International Journal of Protective Structures*, **5**, 367-390. https://doi.org/10.1260/2041-4196.5.4.367

[11] Montanini, R. (2005) Measurement of Strain Rate Sensitivity of Aluminium Foams for Energy Dissipation. *International Journal of Mechanical Sciences*, **47**, 26-42. https://doi.org/10.1016/j.ijmecsci.2004.12.007

[12] Barnat, W., Panowicz, R., Niezgoda, T. and Gieleta, R. (2010) Analysis of a Protective Composite panel with Energy Adsorbent in the Form of Foamed Aluminium. *Journal of Kones*, **17**, 35-44.

[13] Lu, G. and Yu, T. (2003) Energy Absorption of Structures and Materials. Elsevier, Amsterdam. https://doi.org/10.1533/9781855738584

[14] Gibson, L.J. and Ashby, M.F. (1999) Cellular Solids: Structure and Properties. Cambridge University Press, Cambridge.

[15] Reddy, C. J. and Madhu, V. (2017) Dynamic Behaviour of Foams and Sandwich Panels under Shock Wave Loading. *Procedia Engineering*, **173**, 1627-1634. https://doi.org/10.1016/j.proeng.2016.12.260

[16] Baker, W.E., Cox, P., Kulesz, J., Strehlow, R. and Westine, P. (2012) Explosion Hazards and Evaluation. Elsevier, Amsterdam.

[17] Alsubaei, F.C.F. (2015) Performance of Protective Perimeter Walls Subjected to Explosions in Reducing the Blast Resultants on Buildings. Ph.D. Thesis, Western University, London.

[18] Luccioni, B. and Ambrosini, R. (2010) Numerical Assessment of Blast Effects Scaling Procedures. *Mecanica Computacional*, **29**, 1161-1179.

[19] Tiwari, A.K., Tiwary, A.K. and Dhiman, A. (2016) Analysis of Concrete Wall under Blast Loading. *International Journal of Computer Applications*, 12-22.

[20] Lu, Y., Wang, Z. and Chong, K. (2005) A Comparative Study of Buried Structure in

Soil Subjected to Blast Load Using 2D and 3D Numerical Simulations. *Soil Dynamics and Earthquake Engineering*, **25**, 275-288. https://doi.org/10.1016/j.soildyn.2005.02.007

[21] Nurick, G., Gelman, M. and Marshall, N. (1996) Tearing of Blast Loaded Plates with Clamped Boundary Conditions. *International Journal of Impact Engineering*, **18**, 803-827. https://doi.org/10.1016/S0734-743X(96)00026-7

[22] Nurick, G., Chung Kim Yuen, S., Jacob, N., Verster, W., Bwalya, D. and Vara, A. (2006) Response of Quadrangular Mild-Steel Plates to Large Explosive Load. *Proceedings of Second International Conference on Design Analysis of Protective Structures* (*DAPS*), Singapore, 13th-15th November 2006, 30-44.

[23] P. Smith, T. Rose, E. Saotonglang, and CONWEP, (1999) Clearing of Blast Waves from Building Facades. *Proceedings of the Institution of Civil Engineers-Structures and Buildings*, **134**, 193-199. https://doi.org/10.1680/istbu.1999.31385

[24] Igra, O., Wu, X., Falcovitz, J., Meguro, T., Takayama, K. and Heilig, W. (2001) Experimental and Theoretical Study of Shock Wave Propagation through Double-Bend Ducts. *Journal of Fluid Mechanics*, **437**, 255-282. https://doi.org/10.1017/S0022112001004098

[25] Chaudhuri, A., Hadjadj, A., Sadot, O. and Ben-Dor, G. (2013) Numerical Study of Shock-Wave Mitigation through Matrices of Solid Obstacles. *Shock Waves*, **23**, 91-101. https://doi.org/10.1007/s00193-012-0362-2

[26] Nam, J.-W., Yoon, I.-S. and Yi, S.-T. (2016) Numerical Evaluation of FRP Composite Retrofitted Reinforced Concrete Wall Subjected to Blast Load. *Computers and Concrete*, **17**, 215-225. https://doi.org/10.12989/cac.2016.17.2.215

[27] Azmi, M., Kolahchi, R. and Bidgoli, M.R. (2019) Dynamic Analysis of Concrete Column Reinforced with Sio (2) Nanoparticles Subjected to Blast Load. *Advances in Concrete Construction*, **7**, 51-63.

[28] Bentur, S.M.A. (2006) Fibre Reinforced Cementitious Composites. CRC Press, Boca Raton. https://doi.org/10.1201/9781482267747

[29] Shah, S.P. and Rangan, B.V. (1971) Fiber Reinforced Concrete Properties. *Journal Proceeding*, **68**, 126-137. https://doi.org/10.14359/11299

[30] Yoo, D.-Y., Yoon, Y.-S. and Banthia, N. (2015) Predicting the Post-Cracking Behavior of Normal-and High-Strength Steel-Fiber-Reinforced Concrete Beams. *Construction and Building Materials*, **93**, 477-485. https://doi.org/10.1016/j.conbuildmat.2015.06.006

[31] Bruckner, R.O.A. and Curbach, M. (2006) Textile Reinforced Concrete for Strengthening in Bending and Shear. *Materials and Structures*, **39**, 741-748. https://doi.org/10.1617/s11527-005-9027-2

[32] Yoo, D.-Y., Gohil, U., Gries, T. and Yoon, Y.-S. (2016) Comparative Low-Velocity Impact Response of Textile-Reinforced Concrete and Steel-Fiber-Reinforced Concrete Beams. *Journal of Composite Materials*, **50**, 2421-2431. https://doi.org/10.1177/0021998315604039

[33] Wille, K., Naaman, A.E. and Parra-Montesinos, G.J. (2011) Ultra-High Performance Concrete with Compressive Strength Exceeding 150 MPa (22 ksi): A Simpler Way. *ACI Materials Journal*, **108**, 46-54. https://doi.org/10.14359/51664215

[34] Yoo, D.-Y. and Yoon, Y.-S. (2015) Structural Performance of Ultra-High-Performance Concrete Beams with Different Steel Fibers. *Engineering Structures*, **102**, 409-423. https://doi.org/10.1016/j.engstruct.2015.08.029

[35] Lampropoulos, A.P., Paschalis, S.A., Tsioulou, O.T. and Dritsos, S.E. (2016)

Strengthening of Reinforced Concrete Beams Using Ultra High Performance Fibre Reinforced Concrete (UHPFRC). *Engineering Structures*, **106**, 370-384. https://doi.org/10.1016/j.engstruct.2015.10.042

[36] Ng, K.W., Garder, J. and Sritharan, S. (2015) Investigation of Ultra High Performance Concrete pIles for Integral Abutment Bridges. *Engineering Structures*, **105**, 220-230. https://doi.org/10.1016/j.engstruct.2015.10.009

[37] Tanarslan, H.M. (2017) Flexural Strengthening of RC Beams with Prefabricated Ultra High Performance Fibre Reinforced Concrete Laminates. *Engineering Structures*, **151**, 337-348. https://doi.org/10.1016/j.engstruct.2017.08.048

[38] Yang, I.-H., Joh, C., Lee, J.W. and Kim, B.-S. (2013) Torsional Behavior of Ultra-High Performance Concrete Squared Beams. *Engineering Structures*, **56**, 372-383. https://doi.org/10.1016/j.engstruct.2013.05.027

[39] Smith, P. and Hetherington, J. (1994) Blast and Ballistic Loading of Structures Butterworth. Heinemann Ltd, Portsmouth.

[40] Mays, G., Smith, P.D. and Smith, P.D. (1995) Blast Effects on Buildings: Design of Buildings to Optimize Resistance to Blast Loading. Thomas Telford, London.

[41] Conrath, E.J. (1999) Structural Design for Physical Security: State of the Practice. American Society of Civil Engineers, Reston.

[42] Remennikov, A.M. (2002) Blast Resistant Consulting: A New Challenge for Structural Engineers. *Australian Journal of Structural Engineering*, **4**, 121-134. https://doi.org/10.1080/13287982.2002.11464913

[43] Brode, H.L. (1955) Numerical Solutions of Spherical Blast Waves. *Journal of Applied Physics*, **26**, 766-775. https://doi.org/10.1063/1.1722085

[44] Criteria, U.F. (2008) Structures to Resist the Effects of Accidental Explosions. UFC3-340-02, UFC.

[45] Newmark, N. and Hansen, R. (1961) Design of Blast Resistant Structures. In: *Shock and Vibration Handbook*, Vol. 3, McGraw-Hill, New York.

[46] Mills, C. (1987) The Design of Concrete Structure to Resist Explosions and Weapon Effects. *Proceedings of the* 1*st International Conference on Concrete for Hazard Protections*, Edinburgh, 27-30 September 1987, 61-73.

[47] Huson, P. (2012) Experimental and Numerical Simulations of Explosive Loading on Structural Components: Composite Sandwich Connections. Ph. D. Thesis, University of California, San Diego.

[48] Moon, N. (2009) Prediction of Blast Loading and Its Impact on Buildings. Master's Thesis, National Institute of Technology, Trichy.

[49] Khadid, A., Lahbari, N. and Fourar, A. (2007) Blast Loaded Stiffened Plates. *Journal of Engineering and Applied Sciences*, **2**, 456-461.

[50] Le Blanc, G., Adoum, M. and Lapoujade, V. (2005) External Blast Load on Structures–Empirical Approach. *Proceedings of* 5*th European LS-Dyna Users Conference*, Birmingham, 25th-26th May 2005, 1-10.

[51] Pandey, A., Kumar, R., Paul, D. and Trikha, D. (2006) Non-Linear Response of Reinforced Concrete Containment Structure under Blast Loading. *Nuclear Engineering and Design*, **236**, 993-1002. https://doi.org/10.1016/j.nucengdes.2005.09.015

[52] Ngo, T., Mendis, P., Hongwei, M. and Mak, S. (2004) High Strain Rate Behaviour of Concrete Cylinders Subjected to Uniaxial Compressive Impact Loading. *Proceedings of* 18*th Australasian Conference on the Mechanics of Structures and Materials*, Perth, 1-3 December 2004.

[53] Baker, W., Cox, P., Westine, P., Kulesz, J. and Strehlow, R. (1983) Explosion Ha-

zards and Evaluation. Elsevier Scientific Publishing Co., Amsterdam.

[54] Baker, W.E. (1973) Explosions in Air. University of Texas Press, Austin.

[55] Hetherington, J. and Smith, P. (2014) Blast and Ballistic Loading of Structures. CRC Press, Boca Raton. https://doi.org/10.1201/9781482269277

[56] Beshara, F. (1994) Modelling of Blast Loading on Aboveground Structures—I. General Phenomenology and External Blast. *Computers & Structures*, **51**, 585-596. https://doi.org/10.1016/0045-7949(94)90066-3

[57] ASCE (1985) Design of Structures to Resist Nuclear Weapons Effects. Headquarters of the Society, Rome.

[58] Bulson, P.S. (2002) Explosive Loading of Engineering Structures. CRC Press, Boca Raton.

[59] CDG (1945) Structural Defense. British Ministry of Home Security.

[60] Beshara, F. (1994) Modelling of Blast Loading on Aboveground Structures—II. Internal Blast and Ground Shock. *Computers & Structures*, **51**, 597-606. https://doi.org/10.1016/0045-7949(94)90067-1

[61] Lee, E.A. and Seshia, S.A. (2011) Introduction to Embedded Systems—A Cyber-Physical Systems Approach. Second Edition, MIT Press, Cambridge. http://LeeSeshia.org

[62] Biggs, J.M. and Biggs, J.M. (1964) Introduction to Structural Dynamics. McGraw-Hill College, New York.

[63] Ngo, T., Mendis, P., Gupta, A. and Ramsay, J. (2007) Blast Loading and Blast Effects on Structures—An Overview. *Electronic Journal of Structural Engineering*, **7**, 76-91. https://doi.org/10.56748/ejse.671

[64] Grote, D., Park, S. and Zhou, M. (2001) Dynamic Behavior of Concrete at High Strain Rates and Pressures: I. Experimental Characterization. *International Journal of Impact Engineering*, **25**, 869-886. https://doi.org/10.56748/ejse.671

[65] Ceb-Fip, M.C. (1990) Design Code. Comite Euro International du Beton. Thomas Telford, London, 51-59.

[66] Norris, C.H. (1959) Structural Design for Dynamic Loads. McGraw-Hill, New York.

[67] Dowling, A. and Harding, J. (1967) Tensile Properties of Mild Steel under High Strain Rates. *Proceedings of the* 1*st HERF Conference*, Irvine, 1 January 1967.

[68] Malvar, L.J. (1998) Review of Static and Dynamic Properties of Steel Reinforcing Bars. *Materials Journal*, **95**, 609-616. https://doi.org/10.14359/403